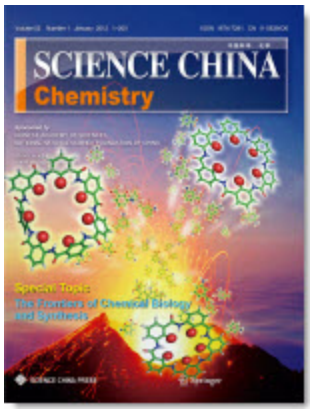

Discriminating G-quadruplex topologies by bright-field microscopy

Journal:	*SCIENCE CHINA Chemistry*
Manuscript ID	SCC-2026-0178.R2
Manuscript Type:	Article
Date Submitted by the Author:	17-Apr-2026
Complete List of Authors:	Zhou, Jun Wei, Shijiong Yan, Xinrong Liu, Bin Qiu, Dehui Mergny, Jean-Louis D , Monchaud Ju, Huangxian; 南京大学化学化工学院,
Keywords:	G-quadruplex, bright-field imaging, particles, aggregation, topology discrimination
Speciality:	Analytical Chemistry

SCIENCE CHINA PRESS

SCIENCE CHINA Chemistry
https://doi.org/10.1007/s11426-xxx-xxxx-x

ARTICLES

Discriminating G-quadruplex topologies by bright-field microscopy

Shijiong Wei [1†], Xinrong Yan [1†], Bin Liu [1], Dehui Qiu [1], Jean-Louis Mergny [1,2], David Monchaud [3], Jun Zhou [1*] & Huangxian Ju[1]

[1]State Key Laboratory of Analytical Chemistry for Life Science, School of Chemistry and Chemical Engineering, Nanjing University, Nanjing 210093, P. R. China
[2]Laboratoire d'Optique et Biosciences (LOB), Ecole Polytechnique, CNRS, INSERM, Institut Polytechnique de Paris, Palaiseau 91120, France
[3]Institut de Chimie Moléculaire de l'Université de Bourgogne (ICMUB), CNRS, UMR6302, Université Bourgogne Europe (UBE), Dijon 21078, France
†Equally contributed to this work.
*Corresponding author(s) (email: jun.zhou@nju.edu.cn)

Received ******; Accepted *****; Published online *****

Abstract G-quadruplexes (G4s) are important regulatory elements for both genetics and epigenetics. Their biological functions mostly rely on their shapes, as a guanine (G)-rich sequence can fold into G4 structures in more than 20 different ways. This shape governs not only their folding kinetics and stability, but also the way G4s interact with cellular effectors, mostly G4-binding proteins. However, there are still some limitations in the simple and reliable identification of G4 topologies. Herein, we propose a novel method relying on the fast formation of G4 topology-dependent particles upon G4 interaction with colistin (COL): monitoring the number, size and shape of these aggregates using a routine bright-field microscope allows for profiling G4 topology in a reliable, inexpensive and user-friendly manner.

Keywords G-quadruplex, bright-field imaging, particles, aggregation, topology discrimination

1 Introduction

G-quadruplexes (G4s) are a class of ubiquitous non-canonical nucleic acid structures prevalent in human cells. To date, more than 1 million potential G4 sequences have been mapped in both the genome and transcriptome [1-3]. This prevalence is illustrated, for instance, by the fact that DNA G4-forming sequences cover *ca*. 1% of the genome [4], and more than 60% of the transcripts contain at least one RNA G4 motif [3]. Owing to their fast-folding kinetics and high stability under physiological conditions [5], the roles that G4s may play in key cellular functions are currently scrutinized. Beyond the control of gene expression and of telomere homeostasis, new roles are uncovered on a regular basis, pertaining to viral infection, aging and age-related diseases for instance. One difficulty in these investigations is that G4s may be transiently folded only [6] and the conditions that control this topological switch, regulated by both the local biological conditions [7] and proteins known to promote their folding/unfolding [8-10], remain to be fully understood.

From a structural point of view, the formation of G4s results from the self-assembly of Gs to form planar, cyclic arrays of four Gs known as G-quartets, which then self-stack (when Gs are consecutive in the G-rich strand) to form the core of a G4 structure [11]. The combination of different structural characteristics—including the nature and length of the loops, their arrangements, the glycosidic angles of the nucleosides, the relative strand orientation, etc.—gives rise to a variety of G4 topologies, as it has been recently shown that a given G4-prone sequence can adopt up to 26 different topologies [12]. Quite conveniently, these different topologies are often classified into three categories, *i.e.*, parallel, antiparallel, and hybrid [11,13]. In addition, the same sequence (*e.g.*, the human telomeric G4) can fold into parallel, hybrid or antiparallel structure (or a mixture of them) as a function of the experimental conditions (*i.e.*, ionic strength, molecular crowding, etc.) [14], which makes it even more difficult to control and/or predict G4 topology [15]. Furthermore, site-specific epigenetic modifications on G4-forming sequences (e.g., DNA methylation) may potentially affect G4 stacking, thereby interfering recognition by intracellular proteins [16,17]. Therefore, rapid and accurate methods for identifying and distinguishing G4 structures are required to understand their functions, yet such methods remain limited.

To discriminate between different G4 topologies, biophysical techniques such as circular dichroism (CD) [18] and thermal difference spectra (TDS) [19], are routinely used, since they are rather simple to implement and reliable. A novel absorbance method was also recently introduced [20]. These spectroscopic methods can be completed by more accurate but low-throughput techniques such as nuclear magnetic resonance (NMR) [21] and X-ray crystallography [22]. It would be interesting to combine the practical convenience of the former three with the accuracy of the latter two: several attempts have been made on the basis of, for instance, nanostructures such as metal-organic frameworks (MOFs) [23] and gold nanoparticles (AuNPs) [24], or of fluorescent G4 probe to discriminate between different G4 folds [25,26]. Although interesting, these methods generally failed to characterize G4 topologies in a simple, reliable and high-throughput manner.

In this work, we report on a novel method based on optical microscopy which leverages the quite unique topology-dependent aggregation of colistin (COL; Figure 1a). We recently demonstrated that COL can selectively interact with G4s and trigger their aggregation without inducing a conformational transition [27]; herein, we aim at further exploiting this property to characterize G4 topologies, showing that COL can be conveniently used to determine G4 topologies through the way the resulting G4/COL complexes aggregate. As further detailed hereafter, this approach allows for a fast, low-cost, and robust identification of the topological nature of the G4 folds. This work provides a constructive method for distinguishing G4 structures and studying the interactions between G4s and other substances.

2 Experimental

Citation: Wei S, Yan X, Liu B, Qiu D, Mergny JL, Monchaud D, Zhou J, Ju H. Discriminating G-quadruplex topologies by bright-field microscopy. *Sci China Chem*, https://doi.org/10.1007/s11426-xxx-xxxx-x

2.1 Materials and reagents

PAGE or HPLC purified DNA oligonucleotides were obtained from Sangon Co., Ltd. (Shanghai, China). Colistin sulfate salt (COL), dimethyl sulfoxide (DMSO), N,N-cacodylic acid (Caco), lithium hydroxide (LiOH), potassium chloride (KCl), thioflavin T (ThT), sodium chloride (NaCl), PEG-200, ammonium persulfate (APS) and *N,N,N′,N′*-tetramethylethylenediamine (TEMED) were purchased from Sigma-Aldrich (MO, USA). All other chemical reagents were obtained from Aladdin (Shanghai, China). All chemical reagents were of analytical grade and used without further purification.

2.2 Preparation of oligonucleotides

DNA concentrations were determined by ultraviolet (UV) spectrometry and the extinction coefficients were obtained by IDT's OligoAnalyzer 3.1. The stock solutions of DNAs were prepared in 10 mM Caco-LiOH buffer (pH 7) with 100 mM KCl. To ensure the formation of stable DNA structures, the DNAs were denatured to 95 °C for 5 min, slowly cooled to room temperature and kept for 2 h, and then stored at 4 °C for subsequent experiments.

In the mixture of COL and DNA, each lysine residue of COL contributes one positive charge, and each DNA phosphate group contributes one negative charge. Hence, the concentrations of negative and positive charges in the mixture are defined as [28]:

$[e^-]$ = [DNA phosphate] = (n-1) × [DNA]

$[e^+]$ = [COL amine] = 5 × [COL]

where "n" is the number of nucleotides, "[DNA]" and "[COL]" denote the concentrations of DNA and COL in the mixture, respectively.

2.3 UV-vis absorption and circular dichroism (CD)

G4 samples were prepared in 10 mM Caco-LiOH buffer (pH 7) containing 100 mM KCl. The CD spectra were collected from 220 to 320 nm (Applied photophysics, UK), and UV-vis spectra were recorded from 220 to 800 nm (Agilent technologies, USA). The change in absorbance at 500 nm (turbidity) of the respective nucleic acid structures was used as an indicator to evaluate the degree of DNA and COL aggregation.

2.4 Confocal laser scanning microscope (CLSM) and wide-field imaging

For specificity experiments, FAM-labeled G4 samples were mixed with COL and incubated for 10 min at room temperature. Subsequently, the mixtures were transferred to hydrophobically treated confocal dishes for imaging. The images were acquired in 100× oil-immersion objective in CLSM and Eclipse Ti2 microscope. The percentage of area coverage (Area %) of the observed structures were quantified according to Equation (1):

$$Area\% = \frac{Area_{particles}}{Area_{view}} \times 100\% \quad \text{(Equation 1)}$$

2.5 Dye staining experiments

To prepare aggregates, G4 (N-myc) was incubated with COL at a charge ratio ($[e^+]/[e^-]$) of 2:1 and a final COL concentration of 20 μM. The mixture was incubated on a hydrophobically treated confocal dish for 10 min at room temperature. Subsequently, the aggregates were stained with either SYBR Gold or ThT [29] and then imaged using an optical microscope.

2.6 Gel electrophoresis analysis

The concentrations of G4 and DNA ladder (T15, T20, and T25) were 1 μM and 5 μM, respectively. The experiments were conducted in 20% native PAGE with 1× Tris-borate-EDTA (TBE) buffer supplemented with 10 mM KCl (to maintain G4 structure). Electrophoresis was run at 150 V for 1.5 h, and followed by staining with SYBR Gold. The PAGE gel was imaged with Gel Doc XR+ imaging system (Bio-Rad, USA).

2.7 Figure preparation and processing

All the plots were generated using Origin and MATLAB software, and the shape descriptors and Area% of particle were calculated by Image J software. The schematic representation was made by BioRender.com. All particle characteristics, including size, area, number, major axis, and minor axis, were quantified using Image J software. For non-monodisperse particle aggregates, images were processed using the "Find Maxima" module. Furthermore, the "Trainable Weka Segmentation" plugin was employed to train a model for rapid image classification. The longest shortest path features were obtained using the "Skeletonization" module.

3 Results and discussion

3.1 Validation and characterization of G4 topology-dependent particles

In previous studies, we discovered that COL can induce G4 aggregation with a preference for parallel over hybrid and antiparallel G4s (Figure 1a,b). Herein, we further investigate the way COL interacts with and precipitates G4s: firstly, turbidity experiments seen in Figures 1c and S1 confirmed that COL-mediated G4 aggregation, monitored *via* measurement of absorbance at 500 nm, is highly efficient with two parallel G4s 2M4P [30] and 2A5P [31] while weaker with antiparallel G4s (2HY9 [32] and 2LOD [33]) and far weaker with hybrid G4s (2KM3 [34] and 7OQT [35]) (Sequences information shown in Figure 1e). To further investigate these interactions, we imaged the particles formed by COL and three different FAM-modified G4s, one of each topology (parallel (PG4), hybrid (HG4) and antiparallel (AG4)) (Figures 1d, S2): interestingly, more particles were formed with PG4s (55) than HG4s (41) and AG4s (11), which is consistent with turbidity studies. Such interesting phenomenon might result from COL binds to the grooves of G4 *via* electrostatic interactions.

Notably, parallel G4 structures exhibit significantly higher affinity for COL than other topologies [27], which may be attributed to their snuggly grooves and more exposed terminal G-quartets facilitating π-π stacking than other topologies. More importantly, COL may function as a "molecular glue" by simultaneously binding to the grooves of two parallel G4s, driving their spontaneous aggregation into particles (Figure S3). The effect of incubation time on particle morphology indicating that the particle morphology reached a stable state after 10 min, without significant changes observed even after 1 hour (Figure S4), which is beneficial to high-throughput analysis. Furthermore, specificity assay revealed that COL exhibits no

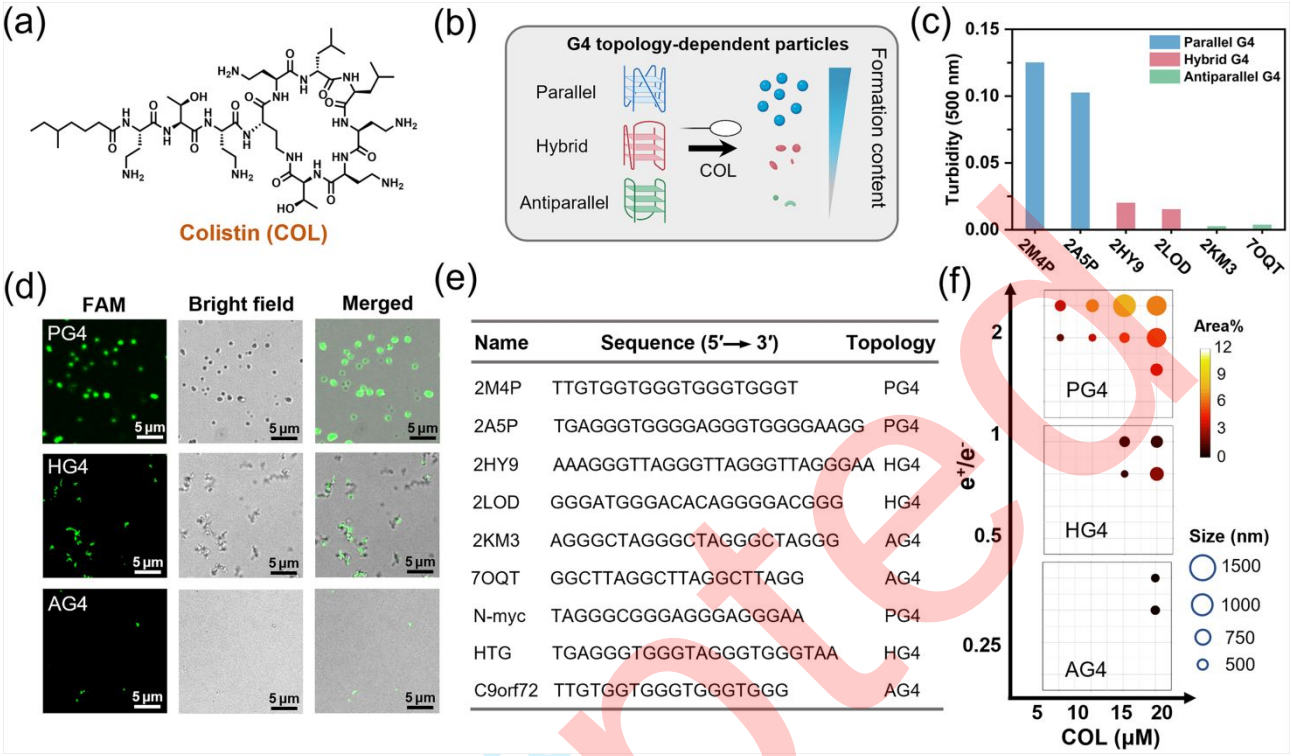

Figure 1 (Color online) Identifying G4 topologies by microscopy. (a) Chemical structure of colistin (COL). (b) Scheme illustration of G4 topology-dependent particles. (c) Turbidity (UV-vis absorbance at 500 nm) of three typical G4 structures, parallel (PG4), hybrid (HG4) and antiparallel (AG4), in the presence of COL. (d) Confocal images of particles made of PG4 (formed by N-myc), HG4 (formed by HTG) and AG4 (formed by C9orf72), and COL (the raw data are presented in Figure S2); the G4 sequences are labelled with FAM at the 5' end, scale bar is 5 μm. (e) DNA sequence used in panels c, d, and f. (f) Particle size and Area% (percentage of the total image area) using G4s with different topologies; the raw data are displayed in Figures S6-S8.

similar aggregation behavior with double-stranded DNA (dsDNA), single-stranded DNA (ssDNA), or i-motif under the same conditions (Figure S5).

Next, we investigated the effect of COL concentration on aggregation by adjusting the charge of COL/DNA mixtures, with a COL concentration varying between 5 and 20 μM, corresponding to a positive-to-negative charge ratio between 0.25 and 2 (DNA concentration ranged from 0.6 to 27.5 μM). The aggregation triggered by PG4s can be observed in the matrix seen in Figure 1f, with a particle size up to 1.3 μm and a coverage density (Area%) up to 6.1%. In sharp contrast, HG4s and AG4s lead to only four and two points in the matrix, respectively, of smaller sizes (<750 nm) and coverage density (Figure 1f). We also observed that PG4s form particles more easily and of sphere-like shapes, while other topologies G4 are rod-like shaped (Figures S6-S9). Even more interesting is the observation that the size and shape differences can be observed by bright-field microscopy (Figure S10), implying that the different G4 topologies can be discriminated using unmodified G4s. Alternatively, the merged images demonstrate that unmodified G4-associated particles can also be stained by SYBR Gold and Thioflavin T (Figure S10), which again show that the particle-based G4 topology discrimination can be realized without covalent labels.

To further exploit this, three G4s were chosen, 2M27, 2JSL and 148D (sequences information are shown in Table S1). Their CD spectra confirm their parallel (2M27), hybrid (2JSL), and antiparallel folds (148D) (Figure 2a). The wide-field images seen in Figure 2b showed COL-induced particles of different shape, number and distribution (Figure S11), as a function of their topology (with the PG4 leading to numerous and larger spherical particles). We then repeated these experiments with 12 different G4s, listed in Table S1, and found that the number and coverage density of obtained particles could be reliably exploited to discriminate between different G4 topologies (Figures 2c, S11, and S12). For instance, the number of particles generated by PG4 2LBY was *ca.* 100-fold higher than that of the AG4 2KF8 (Figure S11). Moreover, this method was also found efficient with mixtures of G4s, for instance, when the HG4 2JSL was mixed with the PG4 1XAV at various ratios (Figure S13): this could be quantified (Figure 2d) and it was found that when the ratio of PG4 *versus* HG4 changed from 100 to 0%, the Area% dropped from 10.3 to 1.1%.

3.2 Classification of different parallel G4s using bright-field imaging

To further monitor the ability of this method to interrogate G4 polymorphism, we used it with eight PG4s (Figure 3a, Table S1), including isolated (*i.e.*, monomeric) G4s, self-stacked (*i.e.*, multimeric) G4s and G4 with nucleobase(s) atop the accessible, external G-quartet (*i.e.*, capped G4s). Multimeric and capped PG4s are usually not discriminated using conventional methods such as CD or gel electrophoresis (Figure 3b). As shown in Figures 3c,d and S14, these PG4s formed with COL aggregates of different shapes (sphere- *versus* string-like particles, which were then categorized parallel 1 and parallel 2, respectively). We then quantified the different features of these aggregates, including the average area, length of the major axis, the number of particles, and our results show the remarkable difference between parallel 1 and parallel 2, the former being monomeric G4s (1XAV, 2LBY, 2M27 and m9T5), while the latter being

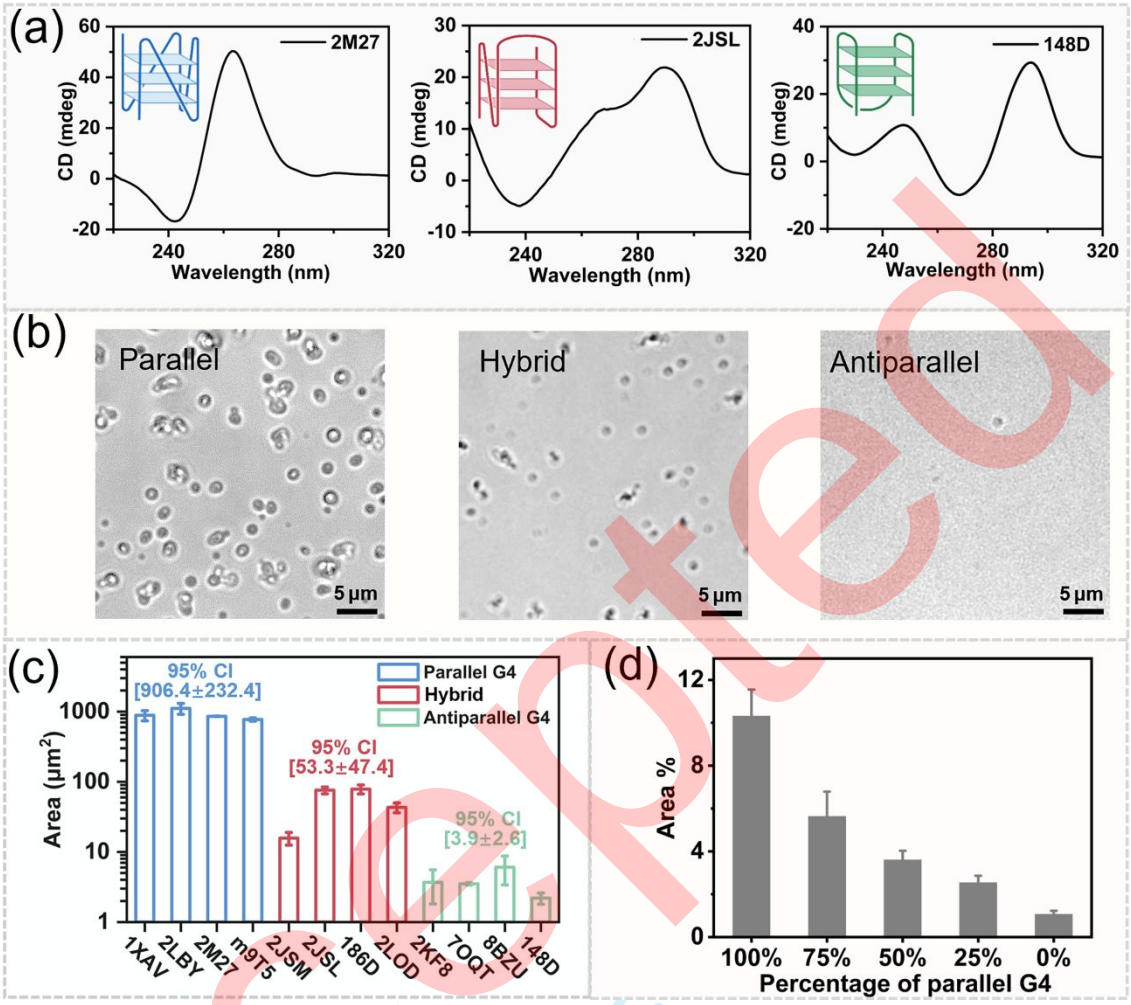

Figure 2 (Color online) Discrimination of G4 topologies: characterization of three G4 topologies using (a) CD spectra and (b) optical microscopy. Three typical G4 structures, parallel G4 (2M27), hybrid (2JSL), and antiparallel (148D) are shown here for comparison. (c) Area (μm^2) covered by different G4s *via* optical microscopy (The confidence interval is 95%); the processed and raw data are shown in Figures S11 and S12, respectively. (d) Plot of Area% for different ratios of parallel G4 (1XAV) to hybrid G4 (2JSL); the raw data are displayed in Figure S13. Note: e^+/e^- = 2, [COL] = 20 μM; scale bar = 5 μm. All the sequences are listed in Table S1.

multimeric ones (2A5P, 2LD8, 2KYP and T30177) (Figures 3e and S15). Gel electrophoresis was performed to confirm their monomeric/multimeric status (Figure S16).

To further demonstrate that the difference in particle size and shape between parallel 1 and parallel 2 originates in their ability to multimerize upon interaction with COL, we used the model PG4 G3T and tuned its multimerization by extending its terminal 3' or 5' length, or both (sequences information displayed in Table S2) [36]. As shown in Figure S17, the presence of one dT tuned the particle shape from string to sphere, which has strong consequences in terms of G4 multimerization, as demonstrated by gel electrophoresis (Figure S18). Spherical particles were obtained with G4s displaying additional Ts on both 5' and 3' ends; however, the influence of the 3' dT on aggregation is higher than that of 5' dT, in agreement with previous results showing that multimerization occurs preferentially on the 3' face [36]. We further studied 2A5P [31] and a 'mutated' sequence (2A5P-5'mut) in which multimerization was hindered by disrupting a base pair near the terminal G-quartet: as shown in Figure S19, when the base pair is hindered in the 5' end of the G4, the shape of the COL-induced particles changed from string to sphere, suggesting that our method can detect an additional base pairs in PG4s. As shown in Figure 3f, our method can thus discriminate both multimeric nature of PG4s and the presence of an additional base pairs in PG4s. However, 2LD8 appears as a monomeric G4 without any capping base pair, and we assume the overhang of G4 hinder the accessibility of π-π stacking under crowding conditions.

3.3 Monitoring of G4 topology conversion

G4 topologies are known to be regulated by crowding environments and flanking sequences [37,38]. The human telomeric repeat $(TTAGGG)_n$ usually serves as a canonical model: for example, its hybrid conformation (2JSM) undergoes a structural transition to a parallel topology (2LD8) under crowding conditions with 40% PEG [39]. To determine whether our method could detect these changes, CD and bright-field imaging experiments were performed: the former confirmed this transition (Figure 4a) and the latter showed that both the number and shape of the COL-induced particles formed by 2JSM are different in the absence (low number and irregular shape) and presence of PEG, which led to numerous, string-like particles (Figure 4b). Interestingly, the transition of particle morphology under different concentrations of PEG also can be observed (Figure S20). The microscopy images thus confirmed that this

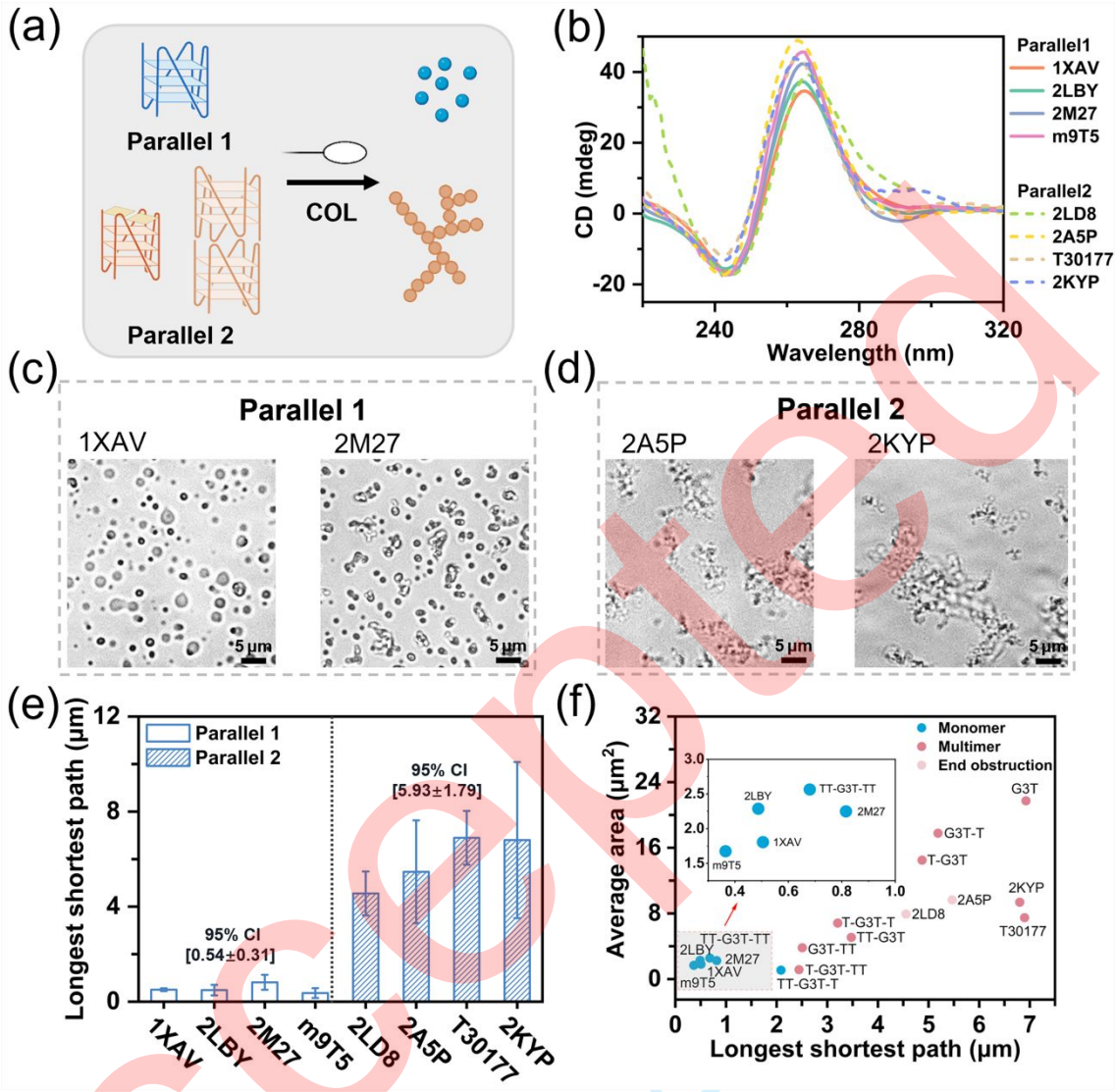

Figure 3 (Color online) Parallel G4 discrimination: (a) COL can aggregate parallel G4 into different shapes for different situation (end capping or multimerization). (b) CD spectra of various parallel G4s. (c,d) Bright field of particles made of (c) parallel 1 and (d) parallel 2 G4s. (e) Longest shortest path (μm) of particles made of different G4s (The confidence interval is 95%); raw and processed data are shown in Figures 3c, d, S14 and S15, respectively. (f) Plot of average area (μm^2) and longest shortest path (μm) of different particles made of parallel G4s; raw data are in Figures 3c, d, S14 and S17. Note: e^+/e^- = 2, [COL] = 20 μM; scale bar = 5 μm.

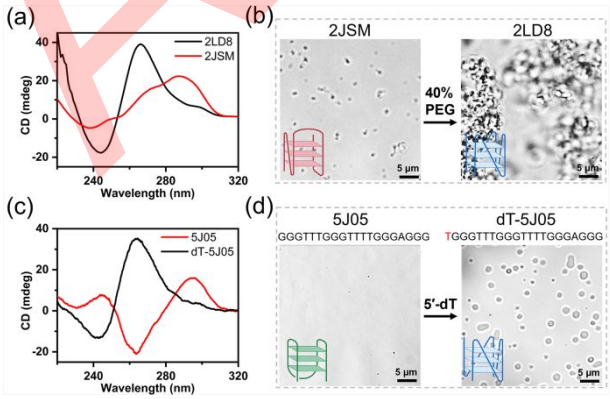

Figure 4 (Color online) Detection of G4 topology transitions using G4-based particles. (a) CD spectra and (b) imaging of G4 topology change induced by molecular crowding. (c) CD spectra and (d) imaging of G4 topology change induced by changing the length of a terminal end. Note: e^+/e^- = 2, [COL] = 20 μM; scale bar = 5 μm.

method is—like CD spectroscopy—responsive to external stimuli-induced topology changes.

We next showed that it is also sensitive to internal stimuli-induced changes, demonstrating that the nature of the flanks can tune the G4 topologies [38]: as seen in Figure 4c, the addition of a T base to the end of the 5J05 sequence changes the topology of its G4 from antiparallel to parallel, and this was reflected by the COL-induced aggregation, as almost no particles were formed with 5J05, in line with their AG4 topology, while those formed with dT-5J05 were spherical, in line with their PG4 nature (Figure 4d).

3.4 Identification of DNA methylation

Finally, we investigated whether our method could be sensitive to DNA methylation, a common epigenetic modification [40] with high frequency at CpG sites [41]. It has been reported that methylation modification affects G4 stacking [42] without affecting the overall G4 topology (notably PG4) [43]. This was

https://www.sciengine.com/doi/10.1007/s11426-026-3488-0
http://chem.scichina.com/english

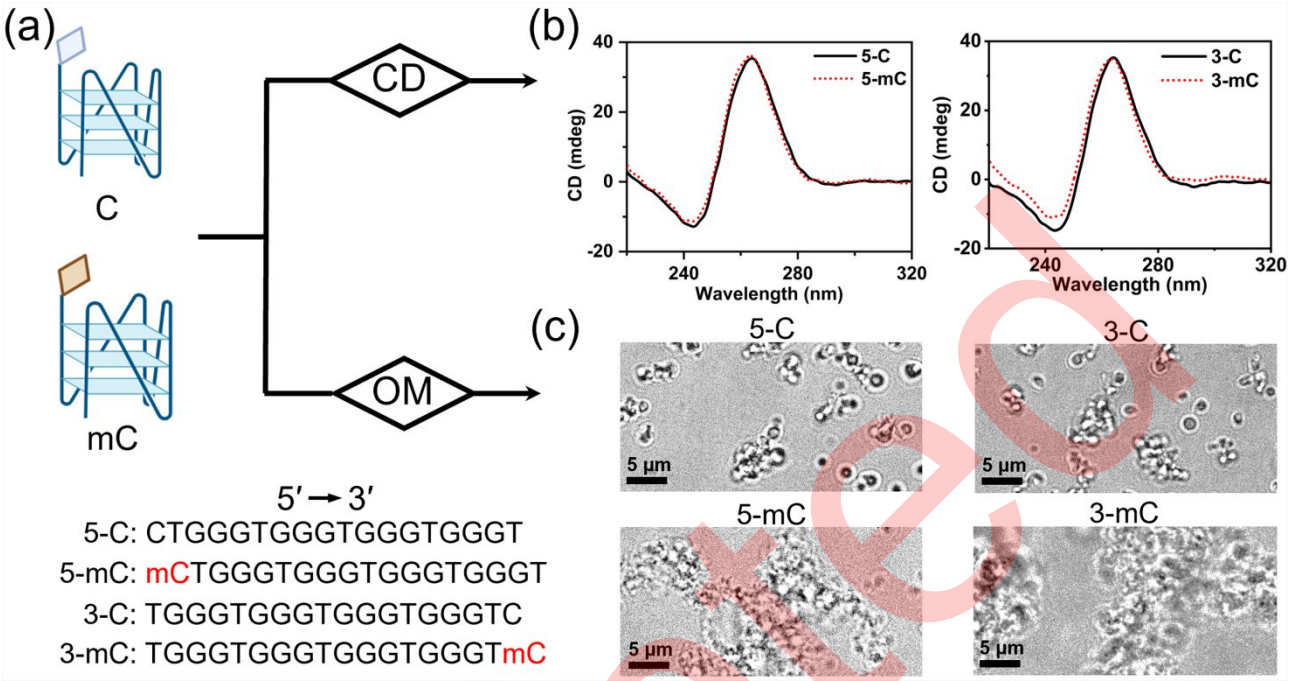

Figure 5 (Color online) G4-based particles reveal the methylation status of a terminal G4 cytosine. (a) 'C' and 'mC' G4s adopt the same parallel topology, which cannot be distinguished by (b) CD spectra but can be readily discriminated by (c) optical microscopy (OM). Note: the concentration of G4 in the CD experiment is 5 μM, while in the optical microscopy (OM) experiments, e^+/e^- = 2, [COL] = 20 μM, and scale bar = 5 μm.

investigated here by CD spectroscopy (Figure 5a, b) but this technique turned out not to be sensitive enough (no significant changes in spectra); in contrast, changing a C to a methylcytosine (mC) led to a change in the shape of COL-induced particles, from spheres to clusters, regardless of whether the mC was located at the 5' or 3' end of the G4 (Figure 5c). The results indicate that the capping base nature strongly influences tetrad accessibility and thus, G4 multimerization. This demonstrates the versatility of our bright-field imaging method, which allows for the precise discrimination of various G4 topologies and is responsive to epigenetic modifications.

4 Conclusions

In summary, G4 topology can be characterized by many techniques, and each of them has its own advantages and disadvantages (Table S3). Herein, we report on a novel technique based on bright-field microscopy, used for the first time to this end, and show that it enables discrimination of G4 topologies based on the number and shape of various COL-induced particles in a very simple and reliable manner. The sensitivity of this method is very high as it can both distinguish different G4 topologies (PG4, HG4 and AG4) and detect subtle structural variations within the same topological family. Interestingly, the necessary nucleic acid amount is very low and the equipment used is widely available in most laboratories, being the simplest microscope possible. In addition, this method is also applicable to RNA G4 recognition, as demonstrated in our previous work [27]. Nevertheless, due to the relatively uniform topology of RNA G4s, we focus mainly on presenting data regarding DNA conformation discrimination. This method is thus fast, inexpensive, reliable and user-friendly, and does not require any DNA/RNA labeling; we thus believe that it is ideally positioned to quickly overtake traditional methods and make the identification of G4 topology readily accessible to all.

Conflict of interest

The authors declare no conflict of interest.

Acknowledgement

We gratefully acknowledge the National Natural Science Foundation of China (22374070, 21977045, 22177047, 22004062, and 22104063), the State Key Laboratory of Analytical Chemistry for Life Science (5431ZZXM2406, and SKLACLS2307), and the Fundamental Research Funds for the Central Universities (202200324, 202200325, and 020514380299).

Supporting Information

The supporting information is available online at http://chem.scichina.com and http://link.springer.com/journal/11426. The supporting materials are published as submitted, without typesetting or editing. The responsibility for scientific accuracy and content remains entirely with the authors.

References

1 Dumas L, Herviou P, Dassi E, Cammas A, Millevoi S. *Trends Biochem Sci*, 2021, 46: 270-283
2 Bedrat A, Lacroix L, Mergny JL. *Nucleic Acids Res*, 2016, 44: 1746-1759
3 Vannutelli A, Belhamiti S, Garant JM, Ouangraoua A, Perreault JP. *NAR Genom Bioinform*, 2020, 2: lqaa035
4 Smeds L, Kamali K, Kejnovská I, Kejnovský E, Chiaromonte F, Makova KD. *Nucleic Acids Res*, 2025, 53: gkaf298
5 You H, Wu J, Shao F, Yan J. *J Am Chem Soc*, 2015, 137: 2424-2427
6 Takahashi S, Kotar A, Tateishi-Karimata H, Bhowmik S, Wang ZF, Chang TC, Sato S, Takenaka S, Plavec J, Sugimoto N. *J Am Chem Soc*, 2021, 143: 16458-16469
7 Nishio M, Tsukakoshi K, Ikebukuro K. *Biosens Bioelectron*, 2021, 178: 113030
8 Mendoza O, Bourdoncle A, Boulé JB, Brosh RM Jr, Mergny JL. *Nucleic Acids Res*, 2016, 44: 1989-2006
9 Lejault P, Mitteaux J, Sperti FR, Monchaud D. *Cell Chem. Biol*, 2021, 28: 436-455
10 Meier-Stephenson V. *Biophys Rev*, 2022, 14: 635-654
11 Mergny JL, Sen D. *Chem Rev*, 2019, 119: 6290-6325
12 Jurkowski M, Kogut M, Olewniczak M, Glinko J, Czub J. *Biophys Rev*, 2025, 129: 9622-9632
13 Dvorkin SA, Karsisiotis AI, Webba da Silva M. *Sci Adv*, 2018, 4: eaat3007
14 Burge S, Parkinson GN, Hazel P, Todd AK, Neidle S. *Nucleic Acids Res*, 2006, 34: 5402-5415
15 Phan AT. *FEBS J*, 2010, 277: 1107-1117
16 Niu K, Xiang L, Zhang X, Li X, Yao T, Li J, Zhang C, Liu J, Peng Y, Xu G, Xiang H, Wang H, Song Q, Feng Q. *Genome Biol*, 2025, 26: 202
17 Medved N, Cevec M, Javornik U, Lah J, Hadži S, Plavec J. *Angew Chem, Int Ed*, 2025, 64: e202507544
18 Vorlíčková M, Kejnovská I, Sagi J, Renčiuk D, Bednářová K, Motlová J, Kypr J. *Methods*, 2012, 57: 64-75
19 Mergny JL, Li J, Lacroix L, Amrane S, Chaires JB. *Nucleic Acids Res*, 2005, 33: e138

20 Largy E, Guédin A, Kabbara A, Mergny JL, Amrane S. *Nucleic Acids Res*, 2025, 53: gkaf953
21 Adrian M, Heddi B, Phan AT. *Methods*, 2012, 57: 11-24
22 Ngo KH, Liew CW, Heddi B, Phan AT. *J Am Chem Soc*, 2024, 146: 13709-13713
23 Peng S, Bie B, Jia H, Tang H, Zhang X, Sun Y, Wei Q, Wu F, Yuan Y, Deng H, Zhou X. *J Am Chem Soc*, 2020, 142: 5049-5059
24 Song T, Wang X, Yao D, Liang H, Lu Y. *Angew Chem Int Ed*, 2022, 61: e202204201
25 Chen J, Hickey BL, Wang L, Lee J, Gill AD, Favero A, Pinalli R, Dalcanale E, Hooley RJ, Zhong W. *Nat Chem*, 2021, 13: 488-495
26 Chen J, Gill AD, Hickey BL, Gao Z, Cui X, Hooley RJ, Zhong W. *J Am Chem Soc*, 2021, 143: 12791-12799
27 Wei S, Zhang X, Feng Y, Tao S, Qiu D, Yan X, Li G, Guittat L, Zhang W, Monchaud D, Mergny JL, Ju H, Zhou J. *J Am Chem Soc*, 2025, 147: 9962-9971
28 Guo W, Ji D, Kinghorn AB, Chen F, Pan Y, Li X, Li Q, Huck WTS, Kwok CK, Shum HC. *J Am Chem Soc*, 2023, 145: 2375-2385
29 Mohanty J, Barooah N, Dhamodharan V, Harikrishna S, Pradeepkumar PI, Bhasikuttan AC. *J Am Chem Soc*, 2013, 135: 367-376
30 Mukundan VT, Phan AT. *J Am Chem Soc*, 2013, 135: 5017-5028
31 Phan AT, Kuryavyi V, Gaw HY, Patel DJ. *Nat Chem Biol*, 2005, 1: 167-173
32 Dai J, Punchihewa C, Ambrus A, Chen D, Jones RA, Yang D. *Nucleic Acids Res*, 2007, 35: 2440-2450
33 Marušič M, Šket P, Bauer L, Viglasky V, Plavec J. *Nucleic Acids Res*, 2012, 40: 6946-6956
34 Lim KW, Alberti P, Guédin A, Lacroix L, Riou JF, Royle NJ, Mergny JL, Phan AT. *Nucleic Acids Res*, 2009, 37: 6239-6248
35 Marquevielle J, De Rache A, Vialet B, Morvan E, Mergny JL, Amrane S. *Nucleic Acids Res*, 2022, 50: 7134-7146
36 Do NQ, Lim KW, Teo MH, Heddi B, Phan AT. *Nucleic Acids Res*, 2011, 39: 9448-9457
37 Xue Y, Kan Zy, Wang Q, Yao Y, Liu J, Hao Yh, Tan Z. *J Am Chem Soc*, 2007, 129: 11185-11191
38 Chen J, Cheng M, Salgado Gilmar F, Stadlbauer P, Zhang X, Amrane S, Guédin A, He F, Šponer J, Ju H, Mergny JL, Zhou J. *Nucleic Acids Res*, 2021, 49: 9548-9559
39 Heddi B, Phan AT. *J Am Chem Soc*, 2011, 133: 9824-9833
40 Peng X, Ma Q, Han D. *Sci China Chem*, 2025, 68: 35-45
41 Xu X, Zeng X, Lin X, Lin S, Liang S, Tian T, Su R, Song J, Yang C. *Sci China Chem*, 2024, 67: 2070-2078
42 Morgan RK, Molnar MM, Batra H, Summerford B, Wadkins RM, Brooks TA. *J Nucleic Acids*, 2018, 2018: 9281286
43 Tsuruta M, Shil S, Taniguchi S, Kawauchi K, Miyoshi D. *Chem Sci*, 2025, 16: 4213-4225